THE JOURNAL OF BIOLOGICAL CHEMISTRY VOL. 284, NO. 46, pp. 32158–32166, November 13, 2009

Single Vesicle Millisecond Fusion Kinetics Reveals Number of SNARE Complexes Optimal for Fast SNARE-mediated Membrane Fusion*[S]

Received for publication, July 21, 2009, and in revised form, August 26, 2009 Published, JBC Papers in Press, September 15, 2009, DOI 10.1074/jbc.M109.047381

Marta K. Domanska[‡], Volker Kiessling[‡], Alexander Stein[§], Dirk Fasshauer[§], and Lukas K. Tamm[‡1]

From the [‡]Center for Membrane Biology and Department of Molecular Physiology and Biological Physics, University of Virginia, Charlottesville, Virginia 22908 and the [§]Department of Neurobiology, Max Planck Institute for Biophysical Chemistry, 37077 Göttingen, Germany

SNAREs mediate membrane fusion in intracellular vesicle traffic and neuronal exocytosis. Reconstitution of membrane fusion *in vitro* proved that SNAREs constitute the minimal fusion machinery. However, the slow fusion rates observed in these systems are incompatible with those required in neurotransmission. Here we present a single vesicle fusion assay that records individual SNARE-mediated fusion events with millisecond time resolution. Docking and fusion of reconstituted synaptobrevin vesicles to target SNARE complex-containing planar membranes are distinguished by total internal reflection fluorescence microscopy as separate events. Docking and fusion are SNAP-25-dependent, require no Ca^{2+}, and are efficient at room temperature. Analysis of the stochastic data with sequential and parallel multi-particle activation models reveals six to nine fast-activating steps. Of all the tested models, the kinetic model consisting of eight parallel reaction rates statistically fits the data best. This might be interpreted by fusion sites consisting of eight SNARE complexes that each activate in a single rate-limiting step in 8 ms.

Neurotransmitter release in synaptic transmission by fusion of synaptic vesicles with the presynaptic membrane is tightly regulated and is probably the fastest membrane fusion event in mammalian cells. Synaptic vesicles are primed and docked to the plasma membrane but do not fuse until triggered by an influx of Ca^{2+} from opened Ca^{2+} channels. After electrical stimulation, neurotransmitter release is observed in less than 1 ms (1–3). The neuronal fusion and disassembly machinery is composed of the soluble *N*-ethylmaleimide-sensitive factor, *N*-ethylmaleimide-sensitive factor attachment proteins (SNAPs),[2] and the SNAP receptors (SNAREs) syntaxin1a (Syx1a), SNAP-25, and synaptobrevin2 (Syb). Proteins such as the Ca^{2+} sensor synaptotagmin, complexin, Sec1/Munc18 homologs, Munc13, and synaptophysin are involved in regulating the fusion process, and Rab GTPases function as upstream tethering factors (4–6). SNARE proteins, which assemble during fusion with equimolar stoichiometry into a parallel four-helix coiled-coil structure with their C termini oriented toward their respective membranes (7–9), play the most essential role in this machinery (10–12). Energy released from a proposed N → C folding process pulls the two membranes together, deforms them, and eventually fuses them in a process that is mechanistically still poorly understood.

SNARE-mediated fusion between target (t)-SNARE (Syx1a and SNAP-25) and vesicle (v)-SNARE (Syb) liposomes has been reconstituted *in vitro* (12). This and many subsequent similar studies were initially criticized because the reaction was very slow (minutes to hours). Adding a C-terminal fragment (residues 49–96) of Syb to the Syx1a/SNAP-25 heterodimer, resulting in a ternary acceptor-SNARE complex, increased the rate of fusion with Syb liposomes by more than an order of magnitude, presumably by preventing the formation of a nonproductive 2:1 Syx1a·SNAP-25 complex (13). However, even this approach did by far not achieve the high fusion rates that are observed in physiological cellular settings. One reason for this remaining discrepancy is that the rate of liposome fusion *in vitro* is dominated by diffusion and docking of cognate SNARE liposomes. To overcome this limitation, several groups including our own have developed single vesicle fusion assays in planar bilayers (14–16). Although they were able to record single fusion events, these earlier studies suffered from several limitations. First, the known physiology and biochemistry was not well reproduced with these earlier preparations. For example, SNAP-25 was not required in the acceptor t-SNARE complex when the assay was performed under very high sensitivity conditions (14, 15) or fusion depended on calcium even in the absence of the calcium sensor synaptotagmin (16). Second, the t-SNARE receptors were reconstituted in the planar membranes with unknown topology and in a laterally immobile form in these membrane preparations. We have now solved both of these problems and present the first single SNARE vesicle fusion events on the millisecond time scale that also reproduce the known physiology of the SNARE fusion system. A detailed kinetic analysis of a large number of single fusion events allowed us to determine the number of productive SNARE complexes that are required to form an active fusion site.

* This work was supported, in whole or in part, by National Institutes of Health Grant P01 GM72694.

[S] The on-line version of this article (available at http://www.jbc.org) contains supplemental Figs. S1–S3 and Movies S1–S5.

[1] To whom correspondence should be addressed. E-mail: Lkt2e@virginia.edu.

[2] The abbreviations used are: SNAP, soluble *N*-ethylmaleimide-sensitive factor attachment protein; SNARE, soluble *N*-ethylmaleimide-sensitive factor attachment protein receptor; Syb, synaptobrevin2; Syx1a, syntaxin1a; t-SNARE, target SNARE; v-SNARE, vesicle SNARE; CHAPS, 3-[(3-cholamidopropyl)dimethylammonio]-1-propanesulfonic acid; TIRF, total internal reflection fluorescence; POPC, 1-palmitoyl-2-oleoyl-phosphatidylcholine; Rh-DOPE, lissamine-rhodamine-B-dioleoylphosphatidylcholine; CDF, cumulative distribution function; p/l, protein/lipid ratio.

EXPERIMENTAL PROCEDURES

Protein Expression and Purification—SNARE proteins from *Rattus norvegicus* cloned in pET28a vector were expressed in BL21(DE3) *Escherichia coli* and purified as described previously (9, 17). The Syx1a construct included residues 183–288 (SyxH3) and SNAP-25A included residues 1–206 with all cysteines replaced by serines. Three Syb constructs were used encompassing residues 49–96, 1–96, and full-length 1–116. In addition, single-cysteine variants of Syb1–96 (Cys^{28}) and SNAP-25 (Cys^{130}) were used. All of the proteins were purified by Ni^{2+}-nitrilotriacetic acid affinity chromatography followed by ion exchange chromatography using MonoQ or MonoS columns. Proteins with transmembrane domains were purified in the presence of 15 mM CHAPS.

The ternary SNARE complex containing SyxH3, SNAP-25, and Syb49–96 (acceptor SNARE complex) and the binary complex containing SyxH3 and SNAP-25 (Syx1a·Syx1a·SNAP-25 complex) were assembled overnight at 4 °C from purified subunits (13). SNARE complexes were additionally purified by MonoQ ion exchange chromatography in the presence of 15 mM CHAPS.

SNARE Reconstitution into Proteoliposomes—Single SNAREs and binary and ternary acceptor SNARE complexes were reconstituted into vesicles by rapid dilution of micellar protein/lipid/detergent mixtures followed by dialysis as described previously (18). Briefly, the desired lipids (including fluorescent probes if needed) were mixed, and organic solvents were evaporated under a stream of N_2 gas followed by vacuum for at least 1 h. The dried lipid films were dissolved with 25 mM sodium cholate in reconstitution buffer (20 mM Hepes, 200 mM KCl, pH 7.4) followed by the addition of an appropriate volume of SNARE proteins to reach a final volume of ~180 μl and the desired protein/lipid ratio. After 1 h of equilibration at room temperature, the mixture was diluted below the critical micellar concentration by adding more reconstitution buffer to a final volume of 550 μl, and the sample was dialyzed overnight against 500 ml of reconstitution buffer at 4 °C with one change of buffer. Protein-free lipid vesicles were prepared by a standard extrusion method as described previously (19).

SNARE Reconstitution into Planar-supported Bilayers—Planar-supported bilayers with reconstituted SNAREs were prepared by a combined Langmuir-Blodgett/vesicle fusion technique as previously described (18–20). Briefly, quartz slides were cleaned by boiling in Contrad detergent for 10 min and hot bath-sonicated while still in detergent for 30 min, followed by extensive rinsing with milliQ water. The slides were then immersed in three volumes of 95% H_2SO_4 to one volume of 30% H_2O_2, followed by extensive rinsing in milliQ water. Immediately before use, the slides were further cleaned for 10 min in an argon plasma sterilizer (Harrick Scientific, Ossining, NY). The first leaflet of the bilayer was prepared by Langumir-Blodgett transfer. To do so, a lipid monolayer was spread from a chloroform solution onto a pure water surface in a Nima 611 Langmuir-Blodgett trough (Nima, Conventry, UK). The solvent was allowed to evaporate for 10 min, before the monolayer was compressed at a rate of 10 cm^2/min to reach a surface pressure of 32 mN/m. After equilibration for 5–10 min, a clean quartz slide was rapidly (200 mm/min) dipped into the trough and slowly (5 mm/min) withdrawn, while a computer maintained a constant surface pressure and monitored the transfer of lipids head groups down onto the hydrophilic substrate.

To complete the bilayer, a solution of proteoliposomes or protein-free vesicles (77 μM total lipid in 1.3 ml, which is a little more than the volume of the holding cell) was added and incubated at room temperature for 2 h. Excess unfused vesicles were then removed by perfusion with 10 ml of reconstitution buffer followed by 5 ml of fusion buffer (20 mM Hepes, 120 mM potassium glutamate, 20 mM potassium acetate, pH 7.4). The quality of the supported bilayers was checked in initial experiments by including labeled proteins and lipids and testing samples for uniformity on a fluorescence microscope and measuring lipid and protein mobility. The bilayer preparations were uniform, and the lipids and most proteins exhibited lateral diffusion coefficients similar to those previously reported (18).

Total Internal Reflection Fluorescence (TIRF) Microscopy—All of the experiments were carried out on a Zeiss Axiovert 35 fluorescence microscope (Carl Zeiss, Thornwood, NY), equipped with a 63× water immersion objective (Zeiss; N.A. = 0.95) and prism-based TIRF illumination. The light source was an argon ion laser (Innova 300C; Coherent, Palo Alto, CA) tuned to 514 nm. Fluorescence was observed through a 610-nm band pass filter (D610/60; Chroma, Brattleboro, VT) by an electron multiplying CCD (DU-860E; Andor Technologies) or a photomultiplier tube (Thorn EMI 9658A; Ruislip). The EMCCD was cooled to −70 °C, and the gain was typically set to an electron gain factor of ~200. The prism-quartz interface was lubricated with glycerol to allow easy translocation of the sample cell on the microscope stage. The beam was totally internally reflected at an angle of 72° from the surface normal, resulting in an evanescent wave that decays exponentially with a characteristic penetration depth of ~100 nm. An elliptical area of 250 × 65 μm was illuminated. The intensity of the laser beam was computer-controlled through an acousto-optic modulator (AOM-40; IntraAction, Bellwood, IL) or could be blocked entirely by a computer-controlled shutter. The laser intensity, shutter, and camera were controlled by a homemade program written in LabVIEW (National Instruments, Austin, TX).

Syb1–96 Binding Assay—Supported bilayers containing acceptor complex (protein/lipid ratio (p/l) of 1:1000) were perfused with 1.5 ml of 0.2 μM Syb1–96_Cys28Alexa546 in fusion buffer on the microscope stage. The binding reaction was monitored for 30 min by TIRF microscopy. Data acquisition was started ~1 min after protein injection, and the fluorescence intensities were recorded every 30 s.

Single Vesicle Docking and Fusion Assay—Supported bilayers containing acceptor SNARE complex (or other proteins as described) were perfused with 3 ml of 0.6 μM Syb1–116 vesicles containing 1 mol % lissamine-rhodamine-B-dioleoylphosphatidylcholine (Rh-DOPE) mixed with 3.3 μM protein-free vesicles in fusion buffer on the microscope stage (concentration refers to total lipid). Data acquisition was started ~1 min after the beginning of vesicle injection. Images of 127 × 127 $pixel^2$ (corresponding to a sample area of 46.7 × 46.7 μm^2) were acquired with an exposure time of 4 ms and a cycle time of 4.01 ms in series of 15,000 images in frame transfer mode and

spooled directly from the CCD camera to the hard drive. Three to five such series were usually collected from each supported membrane preparation. This fast image acquisition period was followed by ~30 min of single image acquisitions every 30 s with 20-ms exposure times to measure additional vesicle docking in bulk mode.

Single Molecule Tracking—A single Cys mutant of SNAP-25 in the 1:1:1 acceptor SNARE complex was labeled in position 130 with Alexa647. Particles were tracked, and diffusion coefficients were determined as described previously (21). The fluorophores were photobleached in single steps. Movies were recorded with 30 frames/s in 1-palmitoyl-2-oleoyl-phosphatidylcholine (POPC) bilayers and 20 frames/s in POPC:cholesterol (4:1) bilayers. No antibleach agents were used in these experiments.

Analysis of Single Vesicle Fusion and Docking Data—The images were analyzed using a homemade program written in LabView (National Instruments). Single vesicles were identified using a previously described single particle tracking algorithm (21). The peak (central pixel) and mean fluorescence intensities of a 5 × 5-pixel^2 area around each identified center of mass were plotted as a function of time for all particles in the 15,000 images of each series.

The mean intensities were extracted from all images after the fast image acquisitions were finished. The mean intensity of single docked vesicles was extracted from the first 10 images in each experiment and used to normalize the data from all images. Experimentally obtained docking curves were fitted with first order kinetics according to Equation 1,

$$D(t) = D_{\infty}[1 - e^{-k_{on}t}] \qquad \text{(Eq. 1)}$$

where D_{∞} is the total concentration of active docking sites, and k_{on} is the docking rate.

RESULTS

The core of the synaptic fusion machinery consists of three proteins: syntaxin1a, SNAP-25, and synaptobrevin2. The process of membrane fusion has been extensively studied both in bulk vesicle fusion assays as well as in supported bilayers. However, numerous questions still remain. In particular, the fusion kinetics and number of complexes required for fusion are still obscure. Here we present a single vesicle-supported membrane fusion assay based on lipid mixing with millisecond time resolution that reveals the kinetics of SNARE-mediated membrane fusion.

Single Vesicle Supported Membrane Fusion Assay

A diagram of the experimental configuration of the single vesicle fusion assay in supported membranes is shown in Fig. 1. To measure docking and fusion of single Rh-DOPE-labeled v-SNARE vesicles to planar t-SNARE membranes by TIRF microscopy, we have reconstituted a preassembled 1:1:1 Syx1a·SNAP-25·Syb49–96 acceptor SNARE complex (13) into planar-supported lipid bilayers composed of POPC and cholesterol (4:1). Experiments with Syx1a only or Syx1a plus subsequently added SNAP-25 did not produce efficient docking and fusion to t-SNARE bilayers (data not shown).

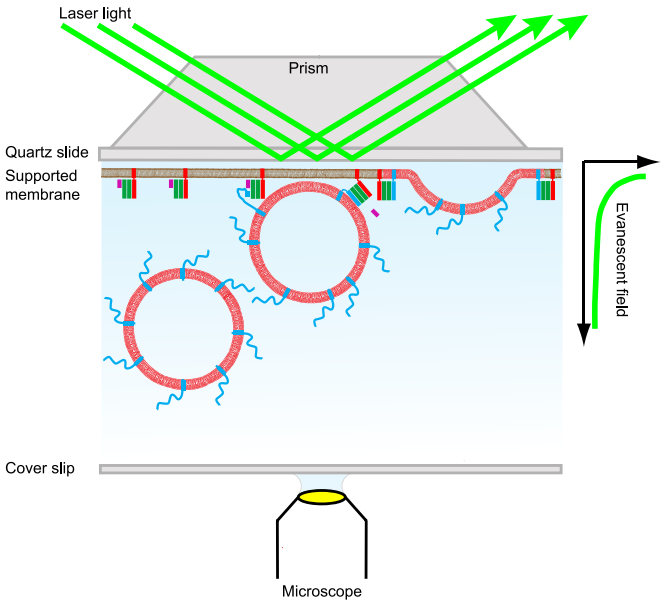

FIGURE 1. **Diagram of the experimental configuration of the single vesicle fusion assay in supported membranes.** The acceptor SNARE complex is unidirectionally reconstituted into a planar-supported bilayer on a quartz microscope slide by a two-step Langmuir-Blodgett/self-assembly process as described under "Experimental Procedures." A water-filled gap exists between the supported membrane and the solid substrate, allowing lipids and most proteins to laterally diffuse in the plane of the membrane. Docking and fusion of synaptobrevin-containing vesicles is observed by TIRF microscopy. The evanescent field penetrates ~100 nm into the solution phase illuminating only docked and fused vesicles but hardly any undocked vesicles.

We have confirmed the activity of reconstituted complexes in supported bilayers (protein/lipid ratio, 1:1000) by binding of soluble Alexa546-labeled synaptobrevin (Syb1–96) peptide (Fig. 2*A*). Upon binding, the shorter Syb49–96 peptide is replaced by the longer Syb1–96 peptide in the complex (13). Binding is specific and reaches half-saturation in 43 ± 3 s. Syb1–96 does not bind to protein-free planar bilayers or membranes with reconstituted Syx1a only (p/l 1:1000).

We have previously reported the reconstitution of a t-SNARE complex in supported bilayers in a laterally mobile form (18). To achieve this, we reconstituted our acceptor SNARE complexes into the planar bilayers by a directed two-step self-assembly process as described under "Experimental Procedures," which results in a right side out SNARE topology (18). In supplemental Movies S1 and S2, we show by single particle tracking that the stabilized 1:1:1 acceptor SNARE complexes used in the current study are also laterally mobile in POPC bilayers without and with cholesterol. The derived diffusion coefficients are 0.68 and 0.14 μm^2/s, respectively.

Docking of v-SNARE Vesicles

We first searched for the optimum protein concentration in our assay. When the acceptor SNARE complex density is varied between 71 and 952 molecules/μm^2 (p/l 1:20,000 to 1:1,500), docking of reconstituted v-SNARE vesicles (Syb1–116; p/l 1:200; POPC:cholesterol 4:1) increases up to ~476 acceptor complexes/μm^2 (p/l 1:3000) (Fig. 2*B*). Prior experiments with different Syb concentrations in the v-SNARE vesicles have established that p/l 1:200, which approximately represents the synaptobrevin density in synaptic vesicles (22), is optimal in

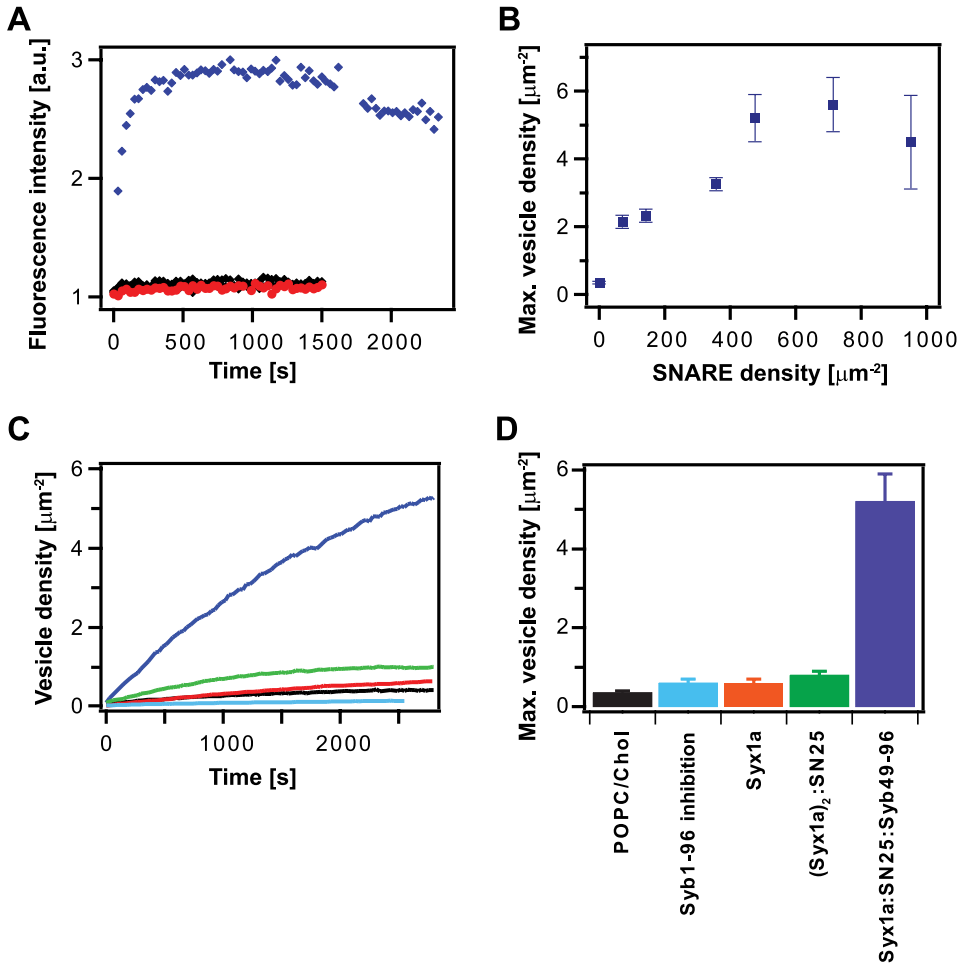

FIGURE 2. **Specific binding of soluble synaptobrevin and docking of synaptobrevin vesicles to acceptor SNARE complex in planar-supported membranes measured by TIRF microscopy.** *A*, binding of Alexa546-labeled Syb1–96 to acceptor SNARE complex (*blue diamonds*), Syx1a only (*red circles*) and protein-free bilayers (*black circles*). The proteins were reconstituted into planar POPC:cholesterol (4:1) membranes at a p/l of 1:1000. *B*, docking of Syb1–116 vesicles to acceptor SNARE complexes as a function of acceptor complex density in the bilayer. Docked vesicle numbers were calculated from the fitted final fluorescence intensities according to Equation 1 and then averaged from 3 to 13 independent experiments. Saturation was reached approximately at a p/l of 1:3000 corresponding to an acceptor density of 467 acceptor SNARE complexes/μm^2 in the membrane. *C*, Syb1–116 vesicle docking curves measured on planar membranes containing acceptor SNARE complex (*blue line*), $(Syx1a)_2$·SNAP-25 complex (*green line*), Syx1a only (*red line*), acceptor SNARE complex preincubated with Syb1–96 (*light blue line*), and on a protein-free lipid bilayer (*black line*). Proteins were reconstituted into planar membranes at p/l of 1:3000. *D*, mean final Syb1–116 vesicle densities after docking to planar membranes containing different target SNAREs at a p/l of 1:3000 as in *C* and averaged from 3 to 13 independent experiments.

liposome fusion (13). Therefore, these t- and v-SNARE concentrations were used in all of the following experiments.

Control experiments showed that docking of v-SNARE vesicles to acceptor SNARE complex-containing bilayers is almost completely inhibited by soluble Syb1–96 (Fig. 2, *C* and *D*, *light blue*), and no docking occurs to protein-free target membranes (Fig. 2, *C* and *D*, *black*). Docking to bilayers containing Syx1a only or $(Syx1a)_2$·SNAP-25 complex is reduced to 11 or 15%, respectively (Fig. 2, *C* and *D*, *red* and *green*). The $(Syx1a)_2$·SNAP-25 complex used in these experiments was prepared by mixing equimolar concentrations of both proteins in detergent followed by an additional purification step. Note that no special attempts were made to push the equilibrium more toward a Syx1a·SNAP-25 complex, for example by using an excess of SNAP-25. It is apparent from these results that efficient docking of v-SNARE vesicles depends on the presence of SNAP-25 and is aided by the presence of the C-terminal Syb peptide that prevents nonproductive 2:1 t-SNARE complex formation (13).

Single Vesicle Fusion

We observed fusion of single v-SNARE vesicles to acceptor SNARE complex-containing supported bilayers by TIRF microscopy (supplemental Movie S3). The mean and peak intensities from each vesicle plotted against time yield traces that can be classified as "docking only" and "docking followed by fusion." Fig. 3 (*A–C*) shows typical examples of docking fusion events with different lag times, Δt_{fus}, between docking and fusion. Fig. 3*D* shows a docking event without progression to fusion. Docking is characterized by a sharp increase of the fluorescence signal. The *arrows* in the *insets* show the onset of fusion, which is defined as the time point when the central pixel (peak) fluorescence intensity starts to decay. Fusion events exhibit a fast drop of the mean intensity because of polarization changes followed by lipid diffusion into the supported bilayer.

Evidence supporting that the fluorescence decays of Fig. 3 represent single fusion events comes from a kinetic analysis of dissipation of Rh-DOPE from the vesicle into the planar membrane. Fig. 4 shows consecutive images of the fusion event presented in Fig. 3*A*. Time point zero was set to the onset of fusion in these graphs, which happened 20 ms after docking in this specific example. The movement of labeled lipids into the supported bilayer can be observed as a dissipating fluorescent cloud in the images in Fig. 4*A*. We extracted the total intensity of the center pixel as well as rings around it with increasing radius and compared them with calculated intensities that would be expected for lateral diffusion from a circular patch of radius 44 nm (approximate vesicle size) in the plane of the membrane and assuming a lipid diffusion coefficient of 1 $\mu m^2/s$. (Fig. 4*B* and supplemental Fig. S1). The intensity of the central pixel (shown in *black*) decays fast, whereas the intensities of rings with 2-pixel (*red*) and 4-pixel (*blue*) radii from the center first increase and then decrease. The experimental data agree very well with the prediction from this very simple lipid diffusion model. When modeling such data, it is critical to take into account the point spread function

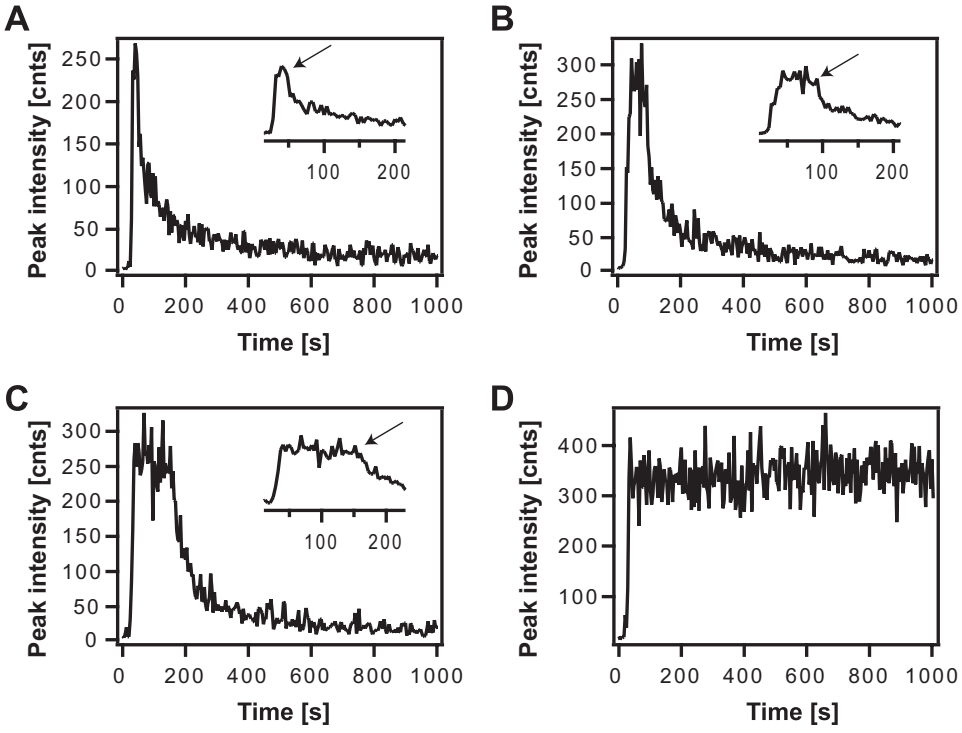

FIGURE 3. **Examples of single Syb1–116 vesicle docking and fusion events to acceptor SNARE complex-containing planar-supported membranes (467 acceptor complexes/μm^2).** Peak fluorescence intensities from each vesicle are plotted as function of time. Time zero is arbitrary for each observed event. The onset of docking time is defined as the mid-point of the sharp rise of each time course. The onset of fusion time is defined as the time (*arrows* in expanded *insets*) when the fluorescence begins to decay to almost zero within a second. Lag times (Δt_{fus}) between docking and fusion were 20 (*A*), 40 (*B*), and 120 ms (*C*) for the three vesicles that fused. The vesicle shown in *D* docked but did not fuse.

describing the experimental resolution of the microscope. We measured the 1/*e* half-width of the point spread function to be 0.25 μm in our system. The small deviations between theory and experiment are most likely caused by vesicle geometry in the evanescent field and polarization effects, which were not included in this calculation.

At 1 mol % Rh-DOPE, we see a rapid initial drop of the fluorescence intensity at the onset of fusion (see supplemental Fig. S1 for details). This can be explained by a reorientation of the fluorophores relative to the evanescent field when a spherical vesicle becomes a more or less flat membrane patch. At higher fluorescent lipid concentrations, this rapid drop is compensated and then superseded by a dequenching peak at the onset of fusion, but this is neither seen nor expected at 1 mol % Rh-DOPE used here.

Control experiments on protein-free bilayers, Syx1a bilayers (supplemental Movie S4) or $(Syx1a)_2$·SNAP-25 complex-containing bilayers (supplemental Movie S5) showed no fusion. Note that we did not optimize our dynamic range for rare or slower fusion rates that may still occur with these much less effective SNARE receptors in the target membrane.

Consistent with expectations from liposome fusion assays (23, 24), but contrary to other reports (16), SNARE-dependent fusion did not require Ca^{2+}. In the presence of 1 mM Ca^{2+}, we did not observe a significant difference in our assay. Examples showing fusion times from two bilayers with and without Ca^{2+} are shown in supplemental Fig. S2. Fusion events occur randomly during long periods of observation (supplemental Fig. S3), which precludes sample heating by laser illumination as contributing to fusion in these experiments.

Kinetic Analysis

1364 single vesicle fusion events from 28 membranes and eight different acceptor complex reconstitutions were analyzed as a function of Δt_{fus}. 43% of all docked vesicles fused, and 63% of these fused within 250 ms after docking. A histogram with a bin size of 4 ms shows that Δt_{fus} is distributed with more than one fraction with distinctive kinetics (Fig. 5*B*). Fig. 5*A* shows the corresponding cumulative distribution function (CDF). Although more fractions with different kinetic rates cannot be excluded, two distributions, one relatively narrow and the other relatively broad, fit the data very well (see below). An initial delay of 10–20 ms before significant fusion happens is apparent in both curves. The sigmoidal shape of the CDF is characteristic for hidden reaction steps that occur before fusion is observable. Such reactions can be modeled by a gamma distribution if several consecutive identical elementary steps lead to observable membrane fusion (25). If the elementary steps occur in parallel, *e.g.* if multiple SNARE complexes are needed to form a single fusion site, a power law like Hodgkin and Huxley's equations describing the gating of ion channels is more appropriate (26). This approach, although on a much slower time scale, has been used before to model kinetic data of influenza hemagglutinin-mediated fusion between pairs of different cells (27).

We consider three models, two parallel and one sequential, to analyze our data. All three models include the observed two fractions of Δt_{fus}. The two parallel models are distinguished by how the two fractions are incorporated.

Parallel Activation: Two Fusion Sites—First, we assume the presence of two different types of fusion sites, which are each characterized by a different number, *m*, of elementary activating particles that activate fusion at different rates, *k* (Fig. 5*C*). The number of fusion events at time *t* then is as follows,

$$N(t) = N_1(1 - e^{-k_1 t})^{m_1} + N_2(1 - e^{-k_2 t})^{m_2} \qquad \text{(Eq. 2)}$$

where *N* is the number of fusion events of a particular fraction, and the subscripts 1 and 2 describe the two fractions.

Parallel Activation: Mixed Fusion Site—In the second model, we assume two fractions of elementary particles that activate at different rates but that are both distributed randomly into all fusion sites (Fig. 5*D*). In this case, the number of quickly activating and slowly activating particles in each fusion site can be described by the following binominal distribution,

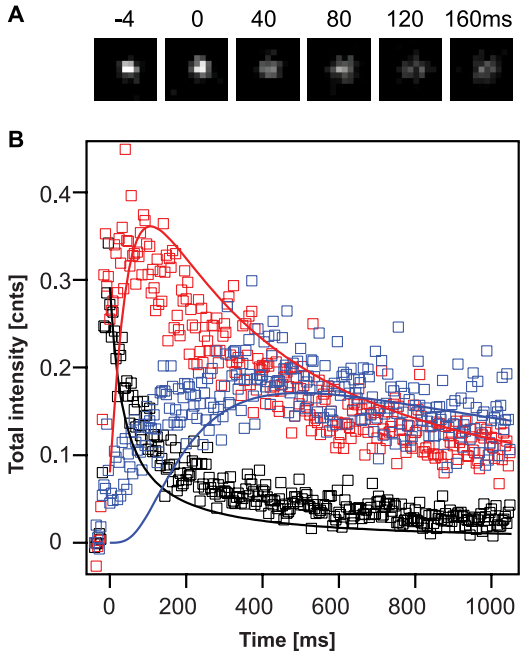

FIGURE 4. **Fusion of a single Rh-DOPE-labeled Syb1–116 vesicle to an acceptor SNARE complex-containing bilayer.** *A*, fluorescence micrographs of a docked vesicle at different time points during fusion showing the dissipation of the fluorescent lipid tracer into the planar membrane. The peak fluorescence intensity trace of this particular vesicle is shown in Fig. 3*A*. Here, time point zero is set to the onset of fusion. *B*, diffusion of Rh-DOPE from the fusion site. Total fluorescence intensities of the central pixel (*black*) and of rings with radii of 2 pixels (0.75 μm) (*red*) and 4 pixels (1.5 μm) (*blue*) from the vesicle center are plotted for the same fusion event as in *A* as a function of time. The *solid lines* are the corresponding theoretically expected intensities from a simulation calculated for lipids that diffuse into the planar bilayer from a 90-nm disk source with a hypothetical diffusion coefficient of 1 $\mu m^2/s$ and taking into account a 1/*e* half-width point spread function of 0.25 μm.

$$N(t) = N\sum_{l=0}^{m}\binom{m}{l}p(1-p)^{m-l}(1-e^{-k_1 t})^{m-l}(1-e^{-k_2 t})^{l} \quad \text{(Eq. 3)}$$

where N is the total number of fusion events, m is the total number of particles in one fusion site, l is the number of particles of fraction 2, and p is the probability of fraction 2. k_1 and k_2 are the activation rates of the fast- and slow-activating particles, respectively.

Sequential Activation: Two Fusion Sites—We also modeled our data with the gamma distribution function for consecutive identical elementary kinetic steps, but with two fractions (Fig. 5*E*). In this case, the number of fusion events at time t is as follows,

$$N(t) = N_1\left(1-\frac{\Gamma(m_1, k_1 t)}{\Gamma(m_1)}\right) + N_2\left(1-\frac{\Gamma(m_2, k_2 t)}{\Gamma(m_2)}\right) \quad \text{(Eq. 4)}$$

where the parameters have the same meaning as in the first model.

The best fit parameters obtained from fits of the histogram and the CDF agreed very well with each other in each of the three models (Fig. 5, *A* and *B*, *solid lines*). Fitting the two independent sites model (Model 1) revealed that 37% of the fusion events required the activation of 9 ± 4 particles to drive fusion at a rate of 131 ± 41 s^{-1}. A slower fraction with a rate of 11 ± 4 s^{-1} required 2 ± 1 particles. The mixed particle fusion site model (Model 2) revealed that active fusion sites are composed of 8 ± 2 particles. 87% of the particles in these sites are activated with a rate of 136 ± 15 s^{-1} with the remainder activated at 10.3 ± 1.2 s^{-1}. The sequential activation model (Model 3) resulted in 37% of fusion events requiring 6 ± 3 activating steps at rates of 295 ± 137 s^{-1} each. The slower activation sites required 2 ± 1 steps that progressed at rates of 14 ± 8 s^{-1}.

Ranking of Fusion Models

We analyzed the quality of each of the fits with Models 1–3 (Figs. 5, *C–E*) by calculating their statistical weights using the Akaike information criteria (28). This analysis revealed that the mixed particle fusion site model (Model 2; Fig. 5*D*) ranks best with an Akaike weight of $w_i = 0.9995$ (calculated for CDF fit and $w_i = 0.79$ for histogram fit), whereas the two fusion site model (model 1; Fig. 5*C*) ranks second with $w_i = 5 \times 10^{-4}$ ($w_i = 0.19$ for histogram fit). The two-site sequential model (Model 3; Fig. 5*E*) reached an Akaike weight of $w_i = 5 \times 10^{-9}$ ($w_i = 0.02$ for histogram fit). Standard χ^2 analysis also ranked Model 2 best, followed by Model 1, and finally by Model 3.

DISCUSSION

Although numerous previous studies established that SNAREs constitute the minimal machinery required for intracellular membrane fusion, an important caveat concerned the speed of fusion, which, at least in synaptic exocytosis, is 5 orders of magnitude faster in cells than in even the fastest reconstituted biochemical systems. Because we are detecting the fusion of single vesicles, the rates of vesicle docking and fusion can be separated in our assay. Docking occurs stochastically over many tens of minutes, essentially for as long as we observe and until all binding sites are saturated (Fig. 2*C*). Individual docking events can only be observed during the first few minutes of each experiment because vesicles eventually dock to higher densities than can be optically resolved, but ensemble docking clearly continues well beyond this stage. Thus, it seems that the "fusion rates" observed in bulk biochemical fusion assays are completely dominated by the docking rates. As expected, the docking of v-SNARE vesicles was dependent on the acceptor SNARE complex density in the target membrane and reached a maximum at 476 acceptor complexes/μm^2 (Fig. 2*B*). This SNARE density is on the same order of magnitude as in the plasma membranes of secretory cells (29). Although our membranes are uniformly fluorescent (lipid or protein labeled), small clusters of syntaxin may exist in the planar membranes as we have recently observed in liposomes with the same lipid composition (30).

Fast Fusion of Single v-SNARE Vesicles Is SNAP-25-dependent, Ca^{2+}-independent, and Efficient at Room Temperature—The fusion times that we observe in our assay are broadly distributed between ~10 and 250 ms with a main peak at 18 ms and a long tail toward longer times (Fig. 5*B*). Although this is still at least 20 times slower than fusion of synaptic vesicles in neurotransmission, it is a huge improvement from the fastest liposome fusion experiments that have been reported *in*

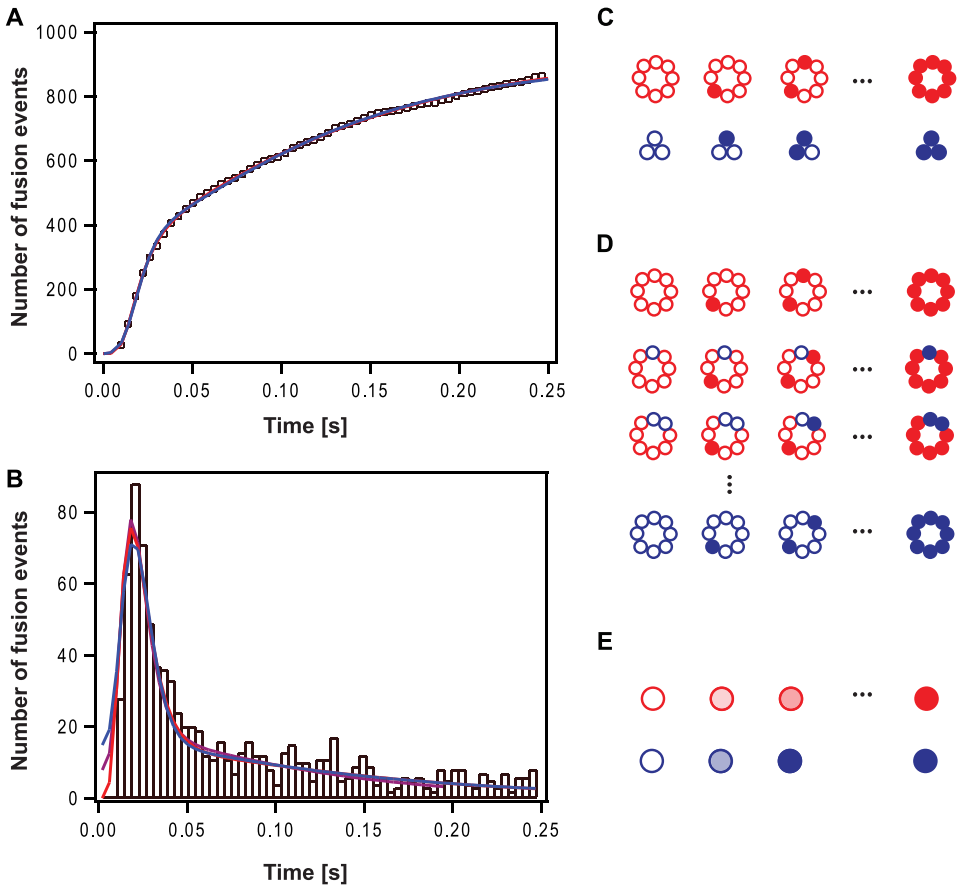

FIGURE 5. **Fusion kinetics of single vesicle SNARE fusion.** *A*, cumulative distribution function of 863 analyzed single Syb1–116 vesicle fusion events to acceptor SNARE complex-containing planar membranes at a density of 467 acceptor complexes/μm. *B*, corresponding histogram of fusion times with a bin size of 4 ms. The data were fitted with three different fusion site models (see text). *Magenta line*, two fusion site model (Model 1); *red line*, mixed fusion site model (Model 2); *blue line*, sequential fusion site model (Model 3). *C–E*, graphic representation of the three models that were tested to interpret the single vesicle fusion kinetic data. The following symbols are used to describe all models: *open circles*, inactive complex; *filled circles*, active complex; *red color*, fast fraction; *blue color*, slow fraction. *C*, two fusion site model (Model 1): two distinct fusion sites (*red* and *blue*) that are each composed of different numbers of particles that are activated randomly at different rates (open-to-filled transition). *D*, mixed fusion site model (Model 2): fusion sites are composed of a fixed total number of particles but may contain different numbers of fast (*red*) and slow (*blue*) randomly activating particles. *E*, sequential fusion site model (Model 3): two distinct fusion sites with different numbers of particles that are activated sequentially with the same rate within the same class (*red* or *blue*) but different rates between the two classes (*red* and *blue*).

vitro (13). Other investigators observed fast fusion in planar bilayer formats (14–16). However, the known physiology and biochemistry of SNARE-driven membrane fusion was not recapitulated in those studies. Fusion was SNAP-25-independent (14, 15), which is in disagreement with numerous *in vivo* and *in vitro* experiments that establish SNAP-25 as an essential t-SNARE component (31–33). Even if spurious fusion between membranes containing only syntaxin and synaptobrevin may be observed under extremely sensitive conditions, the efficiency of fusion should be much greater when SNAP-25 is present in the t-SNARE complex. Indeed, we observe a much greater efficiency of docking and fusion in the presence than in the absence of SNAP-25 in our system. We cannot quantify this efficiency increase because we optimized the dynamic range of our assay to observe large numbers of docking and fusion events with the 1:1:1 acceptor SNARE complex. Under these conditions, we did not observe any fusion events with the 2:1 SNARE complex in a total of 11 min of observation time from a total of five different membranes. Only 37 docking events occurred in this time. When these same conditions were applied to measurements with Syx1a only in the target membrane, we observed only two fusion events in a total of 10 min of observation time from a total of four different membranes. Only 45 docking events occurred in this time.

In another study (16), fusion was only 0.4% efficient without Ca^{2+} but reached 15% efficiency with Ca^{2+}, which should not be the case unless fusion is under the control of the Ca^{2+} sensor synaptotagmin (23, 24). None of these problems compromised our assay, nor was fusion induced by laser heating (14). In fact, we believe it is important to perform the single vesicle fusion assay at a temperature similar to that at which the bilayers were formed. It is well known that both heating and cooling supported bilayers over 10–20 or more degrees cause defects in the membrane (34), which may create artifactual fusion sites. Therefore, the current study is the first to report fast SNARE-driven membrane fusion that is clearly dependent on SNAP-25, requires no Ca^{2+}, and is not induced by thermal changes of the supported membrane.

There are fundamental differences between our and the earlier reconstitutions. First, we use the preassembled acceptor SNARE complex. Syx1a alone, Syx1a plus subsequently added SNAP-25, and preassembled $(Syx1a)_2$·SNAP-25 do not produce efficient docking and fusion in our system. Second, we use a fundamentally different, more gentle method of t-SNARE reconstitution that produces supported membranes with fewer defects (18). In this well controlled method, the first and second monolayers of the bilayer are assembled in two steps, which results in membranes with a right side out SNARE topology (18) and with a controlled transbilayer lipid distribution (35). The lipids and a large fraction of the SNARE proteins are laterally mobile in these preparations (supplemental Movies S1 and S2) (18), which is not the case when the supported bilayers are prepared by simple vesicle adsorption as done in the previous studies (14–16).

Fusion Kinetics Reveals Complex Multicomponent Fusion Reaction—An important result of the present study is the conspicuous delay of fusion after the onset of docking and the resulting sigmoidal shape of the fusion CDF (Fig. 5*A*). This

delay is not due to the time it takes lipids to diffuse out of the observation area because the fluorescent light coming from docked and fusing vesicles actually covers several pixels because of the finite point spread function. The observed fusion delay clearly indicates that several activating steps must occur after docking and before fusion starts. We analyzed our data with three different models. Although the mixed particle binomial distribution site Model 2 fits the data best, all three models essentially agree that approximately six to nine elementary steps activate fusion. The fundamental difference between the three models is that in one extreme these six to nine steps are sequential (Model 3) and in the other extreme they are parallel (Model 2). In the sequential extreme model, the elementary steps might be interpreted as a single SNARE complex undergoing six activation steps, which might include stepwise SNARE complex folding. In the parallel extreme model, the elementary steps most likely represent the formation of approximately eight SNARE complexes needed to form a single fusion site. This parallel reaction scheme rated as the most likely of the three tested models. However, we did not attempt to fit combinations of parallel and serial reaction kinetics. For example, two SNARE complexes might undergo three consecutive activation steps, or four complexes might undergo two consecutive activation steps. A requirement for the applicability of these combinatorial models is that the sequential and parallel rates are of the same order of magnitude. If one or two of these rates were significantly slower than the others, they would become rate-limiting, and the model would revert to the simpler model with the rate-limiting steps. It is also interesting to note that in the parallel Model 1, the slow fusions are mediated by only two activating particles or SNARE complexes. It is therefore possible that the very slow fusions that are observed in the liposome fusion assays are mediated by two SNARE complexes, and the fast fusions that are observed here are mediated by approximately eight SNARE complexes.

SNARE Complex Formation—Another parameter that emerges from these fits is the elementary rate of particle activation. Particle activation, interpreted as N → C folding of single SNARE complexes in the parallel models, takes ~7–8 ms for the fast-activating particles (87% in Model 2) and ~90–100 ms for the slow activating particles (13% in Model 2). In the sequential model, the fast activating elementary steps occur in ~3–4 ms each, and the slow activating steps occur in ~70 ms each. As discussed above for the number of elementary particles in a fusion reaction, a combination of these rates may be possible if the data were interpreted in terms of mixed complex models.

Several groups have previously estimated how many SNARE complexes might constitute a single fusion site, but these estimates were quite indirect and highly variable: blocking dense core granule fusion in permeabilized pheochromocytoma-12 cells with Syb peptides lead to three SNARE complexes/fusion site (36); electrophysiological studies concluded that five to eight SNARE complexes contribute to an entirely proteinaceous fusion pore (37); and dissection of exocytosis with neurotoxins lead to ten to fifteen SNARE complexes/fusion site (38). Our results are consistent with the first two, but not the third of these studies.

Why is fusion in our system still not as fast as in cells? First and foremost, the definition of the fusion time in *in vitro* and in cell physiological experiments is different. In this work, we defined the fusion time as the time from docking to the onset of fusion, whereas in cellular experiments this is usually defined as the time from the arrival of the calcium signal to neurotransmitter release for predocked vesicles. Therefore, strictly speaking, the two are not directly comparable, and the cellular fusion time must always be shorter than the *in vitro* fusion time. Another reason could be that our rates may be slowed by the leaving of the C-terminal Syb peptide from the stabilized acceptor SNARE complex before complete SNARE complex folding and fusion can occur. Based on the random distribution of fusions over the whole measuring time (supplemental Fig. S3), we do not think that vesicle fusion is inhibited by geometric constraints on supported bilayers, at least not up to the first 5 min, from which our data are derived.

As mentioned, it is very likely that synaptic vesicles are docked at the presynaptic membrane in a trigger-ready fashion. For example, the N-terminal part of the SNARE complexes may already be partially folded, but arrested until a cellular signal, *i.e.* Ca^{2+} arrives. This may be accomplished by regulatory proteins such as synaptotagmin, Munc-18, and complexin, which are not present in our reconstitutions. An interesting future extension of this work will be to build these proteins into our system and thereby try to make the assay Ca^{2+}-sensitive and perhaps even faster than what we currently observe. Such a regulated reconstitution assay would offer tremendous new opportunities to further dissect and study how exocytosis is regulated by these proteins, a topic of heated current debates.

REFERENCES

1. Borst, J. G., and Sakmann, B. (1996) *Nature* **383,** 431–434
2. Schneggenburger, R., and Neher, E. (2000) *Nature* **406,** 889–893
3. Wölfel, M., and Schneggenburger, R. (2003) *J. Neurosci.* **23,** 7059–7068
4. Jahn, R., and Scheller, R. H. (2006) *Nat. Rev. Mol. Cell Biol.* **7,** 631–643
5. Malsam, J., Kreye, S., and Söllner, T. H. (2008) *Cell. Mol. Life Sci.* **65,** 2814–2832
6. Rizo, J., and Rosenmund, C. (2008) *Nat. Struct. Mol. Biol.* **15,** 665–674
7. Sutton, R. B., Fasshauer, D., Jahn, R., and Brunger, A. T. (1998) *Nature* **395,** 347–353
8. Poirier, M. A., Xiao, W., Macosko, J. C., Chan, C., Shin, Y. K., and Bennett, M. K. (1998) *Nat. Struct. Biol.* **5,** 765–769
9. Fasshauer, D., and Margittai, M. (2004) *J. Biol. Chem.* **279,** 7613–7621
10. Söllner, T., Whiteheart, S. W., Brunner, M., Erdjument-Bromage, H., Geromanos, S., Tempst, P., and Rothman, J. E. (1993) *Nature* **362,** 318–324
11. Jahn, R., Hanson, P. I., Otto, H., and Ahnert-Hilger, G. (1995) *Cold Spring Harbor Symp. Quant. Biol.* **60,** 329–335
12. Weber, T., Zemelman, B. V., McNew, J. A., Westermann, B., Gmachl, M., Parlati, F., Söllner, T. H., and Rothman, J. E. (1998) *Cell* **92,** 759–772
13. Pobbati, A. V., Stein, A., and Fasshauer, D. (2006) *Science* **313,** 673–676
14. Bowen, M. E., Weninger, K., Brünger, A. T., and Chu, S. (2004) *Biophys. J.* **87,** 3569–3584
15. Liu, T., Tucker, W. C., Bhalla, A., Chapman, E. R., and Weisshaar, J. C. (2005) *Biophys. J.* **89,** 2458–2472
16. Fix, M., Melia, T. J., Jaiswal, J. K., Rappoport, J. Z., You, D., Söllner, T. H., Rothman, J. E., and Simon, S. M. (2004) *Proc. Natl. Acad. Sci. U.S.A.* **101,** 7311–7316
17. Fasshauer, D., Antonin, W., Margittai, M., Pabst, S., and Jahn, R. (1999) *J. Biol. Chem.* **274,** 15440–15446

18. Wagner, M. L., and Tamm, L. K. (2001) *Biophys. J.* **81,** 266–275
19. Wagner, M. L., and Tamm, L. K. (2000) *Biophys. J.* **79,** 1400–1414
20. Kalb, E., Frey, S., and Tamm, L. K. (1992) *Biochim. Biophys. Acta* **1103,** 307–316
21. Kiessling, V., Crane, J. M., and Tamm, L. K. (2006) *Biophys. J.* **91,** 3313–3326
22. Takamori, S., Holt, M., Stenius, K., Lemke, E. A., Grønborg, M., Riedel, D., Urlaub, H., Schenck, S., Brügger, B., Ringler, P., Müller, S. A., Rammner, B., Gräter, F., Hub, J. S., De Groot, B. L., Mieskes, G., Moriyama, Y., Klingauf, J., Grubmüller, H., Heuser, J., Wieland, F., and Jahn, R. (2006) *Cell* **127,** 831–846
23. Bhalla, A., Chicka, M. C., Tucker, W. C., and Chapman, E. R. (2006) *Nat. Struct. Mol. Biol.* **13,** 323–330
24. Stein, A., Radhakrishnan, A., Riedel, D., Fasshauer, D., and Jahn, R. (2007) *Nat. Struct. Mol. Biol.* **14,** 904–911
25. Floyd, D. L., Ragains, J. R., Skehel, J. J., Harrison, S. C., and van Oijen, A. M. (2008) *Proc. Natl. Acad. Sci. U.S.A.* **105,** 15382–15387
26. Hodgkin, A. L., and Huxley, A. F. (1952) *J. Physiol.* **117,** 500–544
27. Blumenthal, R., Sarkar, D. P., Durell, S., Howard, D. E., and Morris, S. J. (1996) *J. Cell Biol.* **135,** 63–71
28. Akaike, H. (1974) *IEEE Transactions on Automatic Control AC* **19,** 716–723
29. Sieber, J. J., Willig, K. I., Kutzner, C., Gerding-Reimers, C., Harke, B., Donnert, G., Rammner, B., Eggeling, C., Hell, S. W., Grubmüller, H., and Lang, T. (2007) *Science* **317,** 1072–1076
30. Murray, D. H., and Tamm, L. K. (2009) *Biochemistry* **48,** 4617–4625
31. Blasi, J., Chapman, E. R., Link, E., Binz, T., Yamasaki, S., De Camilli, P., Südhof, T. C., Niemann, H., and Jahn, R. (1993) *Nature* **365,** 160–163
32. Washbourne, P., Thompson, P. M., Carta, M., Costa, E. T., Mathews, J. R., Lopez-Benditó, G., Molnár, Z., Becher, M. W., Valenzuela, C. F., Partridge, L. D., and Wilson, M. C. (2002) *Nat. Neurosci.* **5,** 19–26
33. Schuette, C. G., Hatsuzawa, K., Margittai, M., Stein, A., Riedel, D., Küster, P., König, M., Seidel, C., and Jahn, R. (2004) *Proc. Natl. Acad. Sci. U.S.A.* **101,** 2858–2863
34. Tamm, L. K., and McConnell, H. M. (1985) *Biophys. J.* **47,** 105–113
35. Crane, J. M., Kiessling, V., and Tamm, L. K. (2005) *Langmuir* **21,** 1377–1388
36. Hua, Y., and Scheller, R. H. (2001) *Proc. Natl. Acad. Sci. U.S.A.* **98,** 8065–8070
37. Han, X., Wang, C. T., Bai, J., Chapman, E. R., and Jackson, M. B. (2004) *Science* **304,** 289–292
38. Montecucco, C., Schiavo, G., and Pantano, S. (2005) *Trends Biochem. Sci.* **30,** 367–372